

# How to infer the shape of the QGP droplet from the data

Magdalena Djordjevic\*,<sup>1</sup> Stefan Stojku,<sup>1</sup> Marko Djordjevic,<sup>2</sup> and Pasi Huovinen<sup>1</sup>

<sup>1</sup>*Institute of Physics Belgrade, University of Belgrade, Serbia*

<sup>2</sup>*Faculty of Biology, University of Belgrade, Serbia*

We propose an approach to extract the spatial anisotropy of QGP formed in ultrarelativistic heavy-ion collisions from measured high- $p_{\perp}$  observables  $R_{AA}$  and  $v_2$ . We show, through analytical arguments, numerical calculations, and comparison with experimental data, that  $v_2/(1 - R_{AA})$  reaches a well-defined saturation value at high  $p_{\perp}$ , and that the initial QGP anisotropy is proportional to this value. With expected future significant reduction of experimental errors, the anisotropy extracted from experimental data will strongly constrain the calculations of initial particle production in heavy-ion collisions and thus test our understanding of QGP physics.

*Introduction:* The major goal of relativistic heavy ion physics [1–4] is understanding the properties of new form of matter called Quark-Gluon Plasma (QGP) [5, 6], which, in turn, allows understanding properties of QCD matter at its most basic level. At the Large Hadron Collider (LHC) and Relativistic Heavy Ion Collider (RHIC) experiments at CERN and Brookhaven National Laboratory (BNL), respectively, QGP is created by colliding heavy ions at ultra-relativistic energies. The created QGP droplet can be of different size, density and shape, depending on the size of the colliding nuclei, and energy and centrality of the collision. In non-central collisions the overlap region of the colliding nuclei has an ellipsoidal shape, and thus in the common experimental setup, in which the colliding nuclei and collision energy are fixed (e.g. in Pb+Pb collisions at  $\sqrt{s_{NN}} = 5.02$  TeV collision energy at the LHC), the centrality of collision defines both the size and shape of the created QGP fireball.

The eccentric shape of the collision system leads to corresponding anisotropy in the azimuthal distribution of final particles (so-called elliptic and triangular flows), where the elliptic flow parameter  $v_2$  is the second Fourier coefficient of the azimuthal distribution of produced particles. The mechanism how the initial spatial anisotropy is converted to final momentum anisotropy is different for low- and high- $p_{\perp}$  particles: For low- $p_{\perp}$  particles, the eccentric shape leads to different pressure gradients to different directions affecting the strength of collective motion to different directions, and thus to azimuthal variation in the particle emission; For high  $p_{\perp}$  particles, eccentricity leads to different paths and consequently different energy losses of high  $p_{\perp}$  jets. While the observed anisotropies of final state particles have an important role in studying the properties of the QCD matter, to extract, say, the shear viscosity coefficient over entropy density ratio  $\eta/s$  from the final state distributions, one must know the initial state anisotropy as well.

However, despite its essential importance, it is still not possible to directly infer the initial anisotropy from experimental measurements. It is possible to measure the anisotropy at the last point of interaction, i.e., at freeze-out using Hanbury-Brown interferometry [7]. Alternatively, one can measure event-by-event fluctuations of the anisotropy by measuring fluctuations of elliptic and triangular flows [8], but it is not possible to measure the average initial state anisotropy.

Several theoretical studies [9–12] have provided different methods for calculating the initial density distribution of the collisions, and thus the initial anisotropy. These approaches however lead to notably different predictions, with their own uncertainties—such uncertainties in the input values have a notable effect in the resulting predictions for both low and high  $p_{\perp}$  data. Since accurate estimate of anisotropy is a major limiting factor for precision QGP tomography, it is evident that alternative approaches for inferring anisotropy are necessary. Optimally, these approaches should be complementary to existing predictions, i.e., based on a method that is fundamentally different to models of early stages of QCD matter.

With this in mind, we here propose a novel approach to extract the initial state anisotropy. Our method is based on inference from *high- $p_{\perp}$*  data, by using already available  $R_{AA}$  and  $v_2$  measurements, which will moreover be measured with much higher precision in the future. Such approach is substantially different from the existing approaches, as it is based on the inference from experimental data (rather than on calculations of early stages of QCD matter), where information from interactions of rare high- $p_{\perp}$  partons with QCD medium are exploited. This also advances the applicability of high  $p_{\perp}$  data to a new level as, up to now, these data were mainly used to study the jet-medium interactions, rather than inferring bulk QGP parameters, such as spatial asymmetry.

*Anisotropy and high  $p_{\perp}$  observables:* In the literature, the initial state anisotropy is quantified in terms

---

\*E-mail: magda@ipb.ac.rs

of eccentricity parameter  $\epsilon_2$

$$\epsilon_2 = \frac{\langle y^2 - x^2 \rangle}{\langle y^2 + x^2 \rangle} = \frac{\int dx dy (y^2 - x^2) \rho(x, y)}{\int dx dy (y^2 + x^2) \rho(x, y)}, \quad (1)$$

where  $\rho(x, y)$  is the initial density distribution of the QGP droplet. The elliptic flow parameter  $v_2$  of high  $p_\perp$  particles is sensitive to both the anisotropy of the system and its size, whereas the nuclear modification factor  $R_{AA}$  is sensitive only to the size of the system [13–16]. It is therefore plausible that the observable to extract eccentricity from high  $p_\perp$  data depends on both  $v_2$  and  $R_{AA}$ .

In [16, 17], we showed that, at very large values of transverse momentum  $p_\perp$ , the fractional energy loss  $\Delta E/E$  (which is otherwise very complex, both analytically and numerically, due to inclusion of multiple effects, see *Numerical results* for more details) shows asymptotic scaling behavior

$$\Delta E/E \sim \chi \langle T \rangle^a \langle L \rangle^b, \quad (2)$$

where  $\langle L \rangle$  is the average path-length traversed by the jet,  $\langle T \rangle$  is the average temperature along the path of the jet,  $\chi$  is a proportionality factor (which depends on initial jet  $p_\perp$ ), and  $a$  and  $b$  are proportionality factors which determine the temperature and path-length dependence of the energy loss. Based on [18–21], we might expect values like  $a = 3$  and  $b = 1$  or  $2$ , but a fit to a full-fledged calculation yields values  $a \approx 1.2$  and  $b \approx 1.4$  [17, 22]. I.e., the temperature dependence of the energy loss is closer to linear, while the length dependence is between linear and quadratic. To evaluate the path length we follow Ref. [23]:

$$L(x, y, \phi) = \frac{\int_0^\infty d\lambda \lambda \rho(x + \lambda \cos(\phi), y + \lambda \sin(\phi))}{\int_0^\infty d\lambda \rho(x + \lambda \cos(\phi), y + \lambda \sin(\phi))}, \quad (3)$$

which gives the path length of a jet produced at point  $(x, y)$  heading to direction  $\phi$ . To evaluate the average path length we take average over all directions and production points.

If  $\Delta E/E$  is small (i.e., for high  $p_\perp$  and in peripheral collisions), we obtain [13, 16, 17]

$$R_{AA} \approx 1 - \xi(\chi) \langle T \rangle^a \langle L \rangle^b. \quad (4)$$

Thus  $1 - R_{AA}$  is proportional to the average size and temperature of the medium. To gauge the anisotropy we define the average path lengths in the in-plane and out-of-plane directions,

$$\begin{aligned} \langle L_{in} \rangle &= \frac{1}{\Delta\phi} \int_{-\Delta\phi/2}^{\Delta\phi/2} d\phi \langle L(\phi) \rangle \\ \langle L_{out} \rangle &= \frac{1}{\Delta\phi} \int_{\pi/2-\Delta\phi/2}^{\pi/2+\Delta\phi/2} d\phi \langle L(\phi) \rangle, \end{aligned} \quad (5)$$

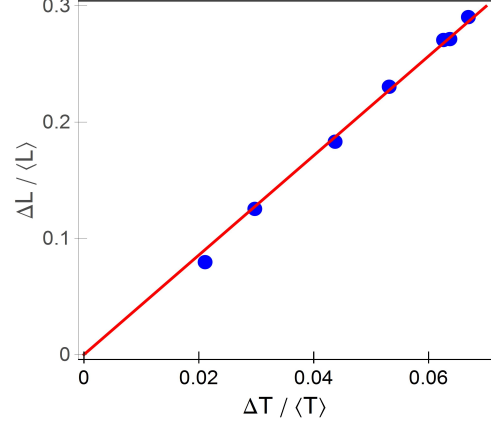


FIG. 1:  $\Delta T/\langle T \rangle$  vs.  $\Delta L/\langle L \rangle$  in Pb+Pb collisions at  $\sqrt{s_{NN}} = 5.02$  TeV collision energy at various centralities [13, 16]. The more peripheral the collision, the larger the values. The red solid line depicts linear fit to the values.

where  $\Delta\phi$  is the acceptance angle with respect to the event plane (in-plane) or orthogonal to it (out-of-plane), and  $\langle L(\phi) \rangle$  the average path length in  $\phi$  direction, while  $\Delta\phi = \pi/6$  [24]. Now we can write  $\langle L \rangle = (\langle L_{out} \rangle + \langle L_{in} \rangle)/2$  and  $\Delta L = (\langle L_{out} \rangle - \langle L_{in} \rangle)/2$ . Similarly, the average temperature along the path length can be split to average temperatures along paths in in- and out-of-plane directions,  $\langle T_{in} \rangle = \langle T \rangle + \Delta T$  and  $\langle T_{out} \rangle = \langle T \rangle - \Delta T$ . When applied to the conventional way to calculate  $v_2$  of high  $p_\perp$  particles [25], we obtain [44]

$$\begin{aligned} v_2 &\approx \frac{1}{2} \frac{R_{AA}^{in} - R_{AA}^{out}}{R_{AA}^{in} + R_{AA}^{out}} \approx \frac{\xi \langle T_{out} \rangle^a \langle L_{out} \rangle^b - \xi \langle T_{in} \rangle^a \langle L_{in} \rangle^b}{4} \\ &\approx \xi \langle T \rangle^a \langle L \rangle^b \left( \frac{b}{2} \frac{\Delta L}{\langle L \rangle} - \frac{a}{2} \frac{\Delta T}{\langle T \rangle} \right), \end{aligned} \quad (6)$$

where we have assumed that  $\xi \langle T \rangle^a \langle L \rangle^b \ll 1$ , and that  $\Delta L/\langle L \rangle$  and  $\Delta T/\langle T \rangle$  are small as well.

By combining Eqs. (4) and (6), we obtain:

$$\frac{v_2}{1 - R_{AA}} \approx \left( \frac{b}{2} \frac{\Delta L}{\langle L \rangle} - \frac{a}{2} \frac{\Delta T}{\langle T \rangle} \right). \quad (7)$$

This ratio carries information on the asymmetry of the system, but through both spatial ( $\Delta L/\langle L \rangle$ ) and temperature ( $\Delta T/\langle T \rangle$ ) variables. Figure 1 shows a linear dependence  $\Delta L/\langle L \rangle \approx c \Delta T/\langle T \rangle$ , where  $c \approx 4.3$ , with the temperature evolution given by one-dimensional Bjorken expansion, as sufficient to describe the early evolution of the system. Eq. (7) can thus be simplified to

$$\frac{v_2}{1 - R_{AA}} \approx \frac{1}{2} \left( b - \frac{a}{c} \right) \frac{\langle L_{out} \rangle - \langle L_{in} \rangle}{\langle L_{out} \rangle + \langle L_{in} \rangle} \approx 0.57\varsigma,$$

$$\text{where } \varsigma = \frac{\langle L_{out} \rangle - \langle L_{in} \rangle}{\langle L_{out} \rangle + \langle L_{in} \rangle} \text{ and } \frac{1}{2} \left( b - \frac{a}{c} \right) \approx 0.57, \quad (8)$$

when  $a \approx 1.2$  and  $b \approx 1.4$ . Consequently, the asymptotic behavior of observables  $R_{AA}$  and  $v_2$  is such that,

at high  $p_{\perp}$ , their ratio is dictated solely by the geometry of the initial fireball. Therefore, the anisotropy parameter  $\varsigma$  can be *directly* extracted from the high- $p_{\perp}$  experimental data.

*Numerical results:* To assess the applicability of the analytically derived scaling in Eq. (8), we calculate  $v_2/(1 - R_{AA})$  using our full-fledged numerical procedure. This procedure is based on our state-of-the-art dynamical energy loss formalism [26, 27], which has several unique features in the description of high- $p_{\perp}$  parton medium interactions: *i)* The formalism takes into account *finite size*, *finite temperature* QCD medium consisting of *dynamical* (that is moving) partons, contrary to the widely used static scattering approximation and/or medium models with vacuum-like propagators (e.g. [18–21]). *ii)* The calculations are based on the finite temperature generalized Hard-Thermal-Loop approach [28], in which the infrared divergencies are naturally regulated [26, 27, 29]. *iii)* Both radiative [26] and collisional [27] energy losses are calculated under *the same* theoretical framework, applicable to both light and heavy flavor. *iv)* The formalism is generalized to the case of finite magnetic [30] mass, running coupling [31] and towards removing widely used soft-gluon approximation [32]. The formalism was further embedded into our recently developed DREENA-B framework [16], which integrates initial momentum distribution of leading partons [33], energy loss with path-length [23] and multi-gluon [34] fluctuations and fragmentation functions [35], in order to generate the final medium modified distribution of high- $p_{\perp}$  hadrons. The framework was recently used to obtain equivalent  $R_{AA}$  and  $v_2$  predictions for 5.02 TeV Pb+Pb collisions at the LHC [16], showing a good agreement with the experimental data.

Our results and the data are shown in Fig. 2. The grey band shows our full DREENA-B result (see above) with the band resulting from the uncertainty in the magnetic to electric mass ratio  $\mu_M/\mu_E$  [36, 37]. The red line corresponds to the  $0.57\varsigma$  limit from Eq. (8), where  $\varsigma$  is the anisotropy of the path lengths used in the DREENA-B calculations [13, 16]. Importantly, for each centrality, the asymptotic regime – where the  $v_2/(1 - R_{AA})$  ratio does not depend on  $p_{\perp}$ , but is determined by the geometry of the system – is already reached from  $p_{\perp} \sim 20\text{--}30$  GeV; the asymptote corresponds to the analytically derived Eq. (8), within  $\pm 5\%$  accuracy. Furthermore, to check if the experimental data support the derived scaling relation, we compare our results to the ALICE [38, 39], CMS [40, 41] and ATLAS [42, 43] data for  $\sqrt{s_{NN}} = 5.02$  TeV  $Pb + Pb$  collisions. The experimental data, for all three experiments, show the same tendency, i.e., the independence on the  $p_{\perp}$  and a consistency with our predictions, though the data error bars are still large. Therefore, from this figure we see that  $v_2/(1 - R_{AA})$  indeed car-

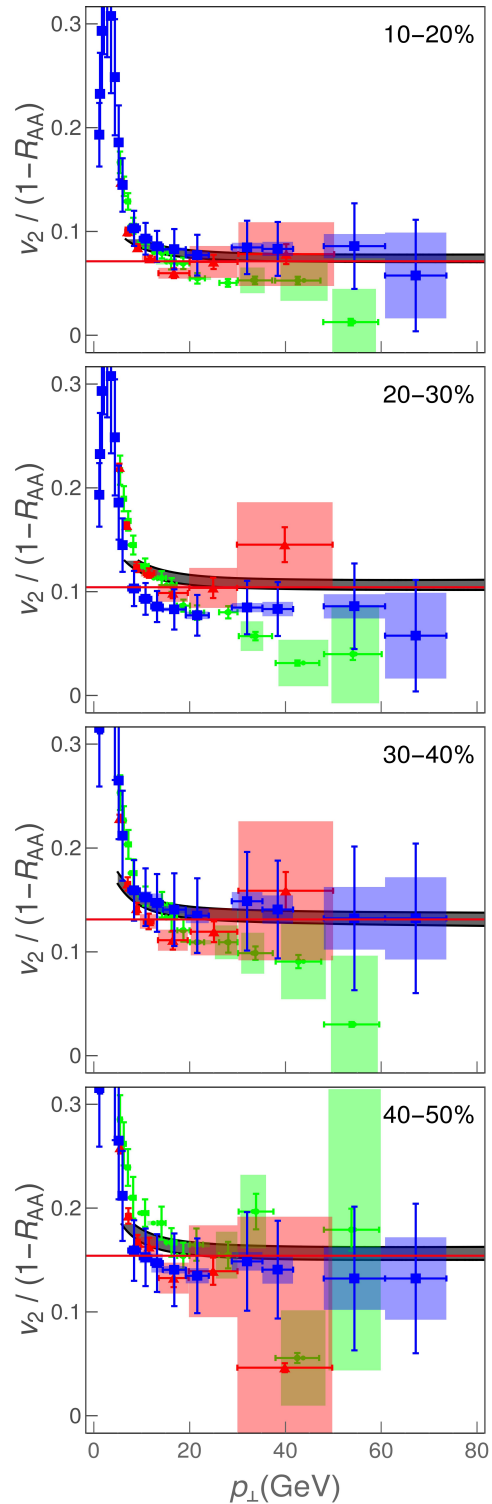


FIG. 2: Theoretical predictions for  $v_2/(1 - R_{AA})$  ratio as a function of transverse momentum  $p_{\perp}$  compared with 5.02 TeV  $Pb + Pb$  ALICE [38, 39] (red triangles), CMS [40, 41] (blue squares) and ATLAS [42, 43] (green circles) data. Panels correspond to 10-20%, 20-30%, 30-40% and 40-50% centrality bins. The gray band corresponds to the uncertainty in the magnetic to electric mass ratio  $\mu_M/\mu_E$ . The upper (lower) boundary of the band corresponds to  $\mu_M/\mu_E = 0.4$  (0.6) [36, 37]. In each panel, the red line corresponds to the limit  $0.57\varsigma$  from Eq. (8).

ries the information about the system's anisotropy, and that this information can be simply (from the straight line high- $p_{\perp}$  limit) and robustly (in the same way for each centrality) inferred from experimental data.

Ideally, the experimental data (here from ALICE, CMS and ATLAS) would overlap with each other, and would moreover have small error-bars. In such a case, the data could be used to directly extract the anisotropy parameter  $\varsigma$  by fitting a straight line to the high- $p_{\perp}$  part of the  $v_2/(1 - R_{AA})$  ratio. While such direct anisotropy extraction would be highly desirable, the available experimental data is unfortunately still far from the level of precision needed to implement this. However, we expect this to change in the upcoming high-luminosity 3<sup>rd</sup> run at the LHC, where the error bars for high- $p_{\perp}$   $R_{AA}$  and  $v_2$  are expected to decrease by almost two orders of magnitude, so that this procedure can be directly applied to experimental data.

It is worth remembering that the anisotropy parameter  $\varsigma$ , which can be extracted from the high- $p_{\perp}$  data, is not the commonly used anisotropy parameter  $\epsilon_2$  (cf. Eqs. (1) and (8)), and if one is known, the other cannot be constructed from that information alone. To facilitate comparison with the  $\epsilon_2$  values in the literature, we construct a high- $p_{\perp}$  proxy

$$\epsilon_{2L} = \frac{\langle L_{out} \rangle^2 - \langle L_{in} \rangle^2}{\langle L_{out} \rangle^2 + \langle L_{in} \rangle^2} = \frac{2\varsigma}{1 + \varsigma^2}. \quad (9)$$

We have checked that for different density distributions  $\epsilon_2$  and  $\epsilon_{2L}$  agree within  $\sim 10\%$  accuracy.

Further, we have extracted the parameters  $\varsigma$  from the DREENA-B results shown in Fig. 2; the corresponding  $\epsilon_{2L}$  results are shown as a function of centrality in Fig. 3 and compared to  $\epsilon_2$  evaluated using various initial state models in the literature [9–12]. Note that conventional (EKRT [10], IP-Glasma [11])  $\epsilon_2$  values trivially agree with our *initial*  $\epsilon_2$  (not shown in the figure) – i.e. the initial  $\epsilon_2$  characterize the anisotropy of the path lengths used as an input to DREENA-B, which we had chosen to agree with the conventional models [45]. It is, however, much less trivial that, through this procedure, in which we calculate the ratio of  $v_2$  and  $1 - R_{AA}$  through full DREENA framework, our *extracted*  $\epsilon_{2L}$  almost exactly recovers our initial  $\epsilon_2$ . Note that  $\epsilon_2$  is *indirectly* introduced in  $R_{AA}$  and  $v_2$  calculations through path-length distributions, while our calculations are performed using full-fledged numerical procedure. Consequently, such direct extraction of  $\epsilon_{2L}$  and its agreement with our initial (and consequently also conventional)  $\epsilon_2$  is highly non-trivial and gives us a good deal of confidence that  $v_2/(1 - R_{AA})$  presents a reliable observable for anisotropy inference. Additional important feature of Fig. 3 is that the width of the  $\epsilon_{2L}$  band is smaller than the difference in the  $\epsilon_2$  values obtained by using different models (especially MC-Glauber [9] vs. MC-KLN [12] models). Thus, our

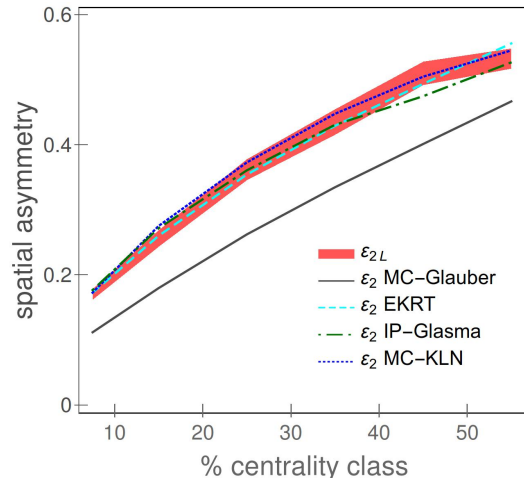


FIG. 3: Comparison of  $\epsilon_{2L}$  (red band) obtained from our method, with  $\epsilon_2$  calculated using Monte-Carlo (MC) Glauber [9] (gray band), EKRT [10] (the purple band), IP-Glasma [11] (green dot-dashed curve) and MC-KLN [12] (blue dotted curve) approaches. MC-Glauber and EKRT results correspond to 5.02 TeV, while IP-Glasma and MC-KLN correspond to 2.76 TeV  $Pb + Pb$  Collisions at the LHC.

approach provides genuine resolving power to distinguish between different initial state models, although it may not be possible to distinguish the finer details separating the more sophisticated models, i.e., EKRT [10] and IP-Glasma [11]. As mentioned,  $\epsilon_{2L}$  and  $\epsilon_2$  slightly differ, and thus we propose that the practitioners of the initial state models should calculate not only  $\epsilon_2$  (and higher order anisotropies), but  $\epsilon_{2L}$  or  $\varsigma$  as well.

*Summary:* High- $p_{\perp}$  theory and data are traditionally used to explore interactions of traversing high- $p_{\perp}$  probes with QGP, while bulk properties of QGP are obtained through low- $p_{\perp}$  data and the corresponding models. On the other hand, it is clear that high- $p_{\perp}$  probes are also powerful tomography tools since they are sensitive to global QGP properties. We here demonstrated this in the case of spatial anisotropy of the QCD matter formed in ultrarelativistic heavy-ion collisions. We used our dynamical energy loss formalism to show that a (modified) ratio of two main high- $p_{\perp}$  observables,  $R_{AA}$  and  $v_2$ , presents a robust observable for straightforward extraction of a parameter characterizing the anisotropy. We analytically estimated the proportionality between  $v_2/(1 - R_{AA})$  ratio and anisotropy coefficient  $\epsilon_{2L}$ , and found surprisingly good agreement with full-fledged numerical calculations and conventional  $\epsilon_2$  values. The experimental accuracy does not yet allow the extraction of the anisotropy from the data using our scheme, but once the accuracy improves in the upcoming LHC runs as expected, the anisotropy of the QGP formed in heavy ion collisions can be inferred directly from the data. Such

experimentally obtained anisotropy parameter would provide an important constraint to models describing the early stages of heavy-ion collision and QGP formation, and demonstrate synergy of high- $p_{\perp}$  theory and data with more common approaches for inferring QGP properties.

**Acknowledgments:** We thank Jussi Auvinen, Hendrik van Hees, Etele Molnar and Dusan Zigic for useful discussions. We also thank Tetsufumi Hirano and Harri Niemi for sharing their MC-KLN and EKRT results with us. This work is supported by the European Research Council, grant ERC-2016-COG: 725741, and by the Ministry of Science and Technological Development of the Republic of Serbia, under project numbers ON171004 and ON173052.

- 
- [1] M. Gyulassy and L. McLerran, Nucl. Phys. A **750**, 30 (2005).
- [2] E. V. Shuryak, Nucl. Phys. A **750**, 64 (2005).
- [3] B. Jacak and P. Steinberg, Phys. Today **63**, 39 (2010).
- [4] C. V. Johnson and P. Steinberg, Physics Today **63**, 29 (2010).
- [5] J. C. Collins and M. J. Perry, Phys. Rev. Lett. **34**, 1353 (1975).
- [6] G. Baym and S. A. Chin, Phys. Lett. B **62**, 241 (1976).
- [7] L. Adamczyk *et al.* [STAR Collaboration], Phys. Rev. C **92**, no. 1, 014904 (2015).
- [8] H. Niemi, G. S. Denicol, H. Holopainen and P. Huovinen, Phys. Rev. C **87**, no. 5, 054901 (2013).
- [9] C. Loizides, J. Kamin, D. d’Enterria, Phys. Rev. C **97**, 054910 (2018).
- [10] K. J. Eskola, H. Niemi, R. Paatelainen and K. Tuominen, Phys. Rev. C **97**, no. 3, 034911 (2018).
- [11] J. E. Bernhard, J. S. Moreland, S. A. Bass, J. Liu and U. Heinz, Phys. Rev. C **94**, no. 2, 024907 (2016).
- [12] T. Hirano, P. Huovinen, K. Murase and Y. Nara, Prog. Part. Nucl. Phys. **70**, 108 (2013).
- [13] D. Zigic, I. Salom, J. Auvinen, M. Djordjevic and M. Djordjevic, arXiv:1805.03494 [nucl-th].
- [14] T. Renk, Phys. Rev. C **85**, 044903 (2012).
- [15] D. Molnar and D. Sun, Nucl. Phys. A **932**, 140 (2014); Nucl. Phys. A **910-911**, 486 (2013).
- [16] D. Zigic, I. Salom, J. Auvinen, M. Djordjevic and M. Djordjevic, Phys. Lett. B **791**, 236 (2019).
- [17] M. Djordjevic, D. Zigic, M. Djordjevic, J. Auvinen, arXiv:1805.04030 [nucl-th].
- [18] R. Baier, Y. Dokshitzer, A. Mueller, S. Peigne, and D. Schiff, Nucl.Phys.B **484**, 265 (1997).
- [19] N. Armesto, C. A. Salgado, and U. A. Wiedemann, Physical Review D **69**, 114003 (2004).
- [20] M. Gyulassy, P. Lvai, and I. Vitev, Nuclear Physics B **594**, 371 (2001).
- [21] W. Xin-Nian and X. Guo, Nuclear Physics A **696** (2001).
- [22] M. Djordjevic and M. Djordjevic, Phys. Rev. C **92**, 024918 (2015).
- [23] A. Dainese [ALICE Collaboration], Eur. Phys. J. C **33**, 495 (2004).
- [24] S. Afanasiev *et al.* [PHENIX Collaboration], Phys. Rev. C **80**, 054907 (2009).
- [25] P. Christiansen, K. Tywoniuk and V. Vislavicius, Phys. Rev. C **89**, no. 3, 034912 (2014).
- [26] M. Djordjevic, Phys. Rev. C **80**, 064909 (2009); M. Djordjevic and U. Heinz, Phys. Rev. Lett. **101**, 022302 (2008).
- [27] M. Djordjevic, Phys. Rev. C **74**, 064907 (2006).
- [28] J. I. Kapusta, *Finite-Temperature Field Theory* (Cambridge University Press, 1989).
- [29] M. Djordjevic and M. Gyulassy, Phys. Rev. C **68**, 034914 (2003).
- [30] M. Djordjevic and M. Djordjevic, Phys. Lett. B **709**, 229 (2012).
- [31] M. Djordjevic and M. Djordjevic, Phys. Lett. B **734**, 286 (2014).
- [32] B. Blagojevic, M. Djordjevic and M. Djordjevic, arXiv:1804.07593 [nucl-th].
- [33] Z. B. Kang, I. Vitev and H. Xing, Phys. Lett. B **718**, 482 (2012).
- [34] M. Gyulassy, P. Levai and I. Vitev, Phys. Lett. B **538**, 282 (2002).
- [35] D. de Florian, R. Sassot and M. Stratmann, Phys. Rev. D **75**, 114010 (2007).
- [36] Yu. Maezawa *et al.* [WHOT-QCD Collaboration], Phys. Rev. D **81** 091501 (2010).
- [37] A. Nakamura, T. Saito and S. Sakai, Phys. Rev. D **69**, 014506 (2004).
- [38] S. Acharya *et al.* [ALICE Collaboration], JHEP **1811**, 013 (2018).
- [39] S. Acharya *et al.* [ALICE Collaboration], JHEP **1807**, 103 (2018).
- [40] V. Khachatryan *et al.* [CMS Collaboration], JHEP **1704**, 039 (2017).
- [41] A. M. Sirunyan *et al.* [CMS Collaboration], Phys. Lett. B **776**, 195 (2018).
- [42] [ATLAS Collaboration], ATLAS-CONF-2017-012.
- [43] M. Aaboud *et al.* [ATLAS Collaboration], Eur. Phys. J. C **78**, no. 12, 997 (2018).
- [44] Note that the first approximate equality in Eq. (6) can be shown to be exact if the higher harmonics  $v_4$ ,  $v_6$ , etc., are zero, and the opening angle where  $R_{AA}^{in}$  and  $R_{AA}^{out}$  are evaluated is zero (cf. definitions of  $\langle L_{out} \rangle$  and  $\langle L_{in} \rangle$ , Eq. (5)).
- [45] Binary collision scaling calculated using optical Glauber model with additional cut-off in the tails of Woods-Saxon potentials, to be exact.